

## The Power of $\alpha$ — Errata

*Malcolm H. Macgregor*

**p. 12, Fig. 0.1.12:**

Interchange the following data-point labels:

$$D^0 \rightarrow D_s^+, D_s^+ \rightarrow B_c^+, B_c^+ \rightarrow D^0$$

**p. 90, Table 2.1.1:**

Line 2 of caption should read “1 zs =  $10^{-21}$  sec”

**p. 106:**

Line 13 should read “ratio is 4.1”

**p. 127:**

Line 4 up from bottom should read “ $\Sigma^-$  baryons”

**p. 136, Fig. 2.9.1:**

Interchange the following data-point labels:

$$D^0 \rightarrow D_s^+, D_s^+ \rightarrow B_c^+, B_c^+ \rightarrow D^0$$

**p. 139, Fig. 2.10.1:**

Line 8 of caption should read “particles that contain”

**p. 209:**

Line 13 of text, delete “ $M^X$ ”

**p. 229, Fig. 3.17.2:**

Line 8 of caption should read “( $q \equiv u, d$ )”

**p. 235, Fig. 3.18.1:**

Delete the energy scale at the left

**p. 289:**

Line 30 should read “...in Fig. 0.2.20... . Two  $M_K$ ”

**p. 306, Table 4.3.1:**

Delete Corollary C

**p. 354:**

Line 25 should read “(Sec. 3.26)”

**p. 354:**

Line 35 should read “ $q^\alpha \equiv (u^\alpha, d^\alpha) = q/\alpha \equiv (u, d)/\alpha$ ”

---

For additional information go to the following websites:

**WS:** <http://www.worldscibooks.com/physics/6213.html>

**MHM:** [70mev.org](http://70mev.org) or [powerofalpha.org](http://powerofalpha.org)

---

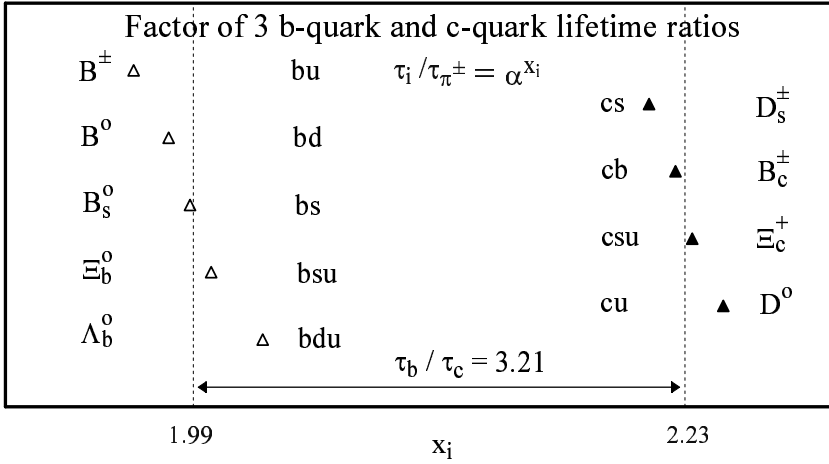


**Fig. 0.1.12** The factor-of-3 flavor structure which exists between the five unpaired  $b$ -quark states (which require no HF corrections) and the four unpaired  $c$ -quark states that require no HF corrections. The group-averaged lifetime ratio between these two groups is 3.21, with the higher-mass  $b$ -quark states having the longer lifetimes. The corresponding  $(\Upsilon_{1S} \equiv b\bar{b}) / (J/\Psi_{1S} \equiv c\bar{c})$  mass ratio is 3.05 (Fig. 2.9.2). The lifetime ratio between the  $B_s^0 \equiv bs$  and  $D_s^\pm \equiv cs$  mesons, where a  $b$  quark is replaced by a  $c$  quark, is 2.99.

$c$ -quark particles. We ordinarily expect the heavier unstable particles to decay faster than the lighter ones, but the opposite situation applies here. An interesting point is that the deviation of the  $c$ -quark states from the lifetime  $\alpha$ -grid is not random, but is characteristically a factor of 3, so that we have in effect another type of HF lifetime fine structure. Perhaps the most interesting point historically is that the  $b$ -quark lifetimes, which were measured almost two decades after this lifetime  $\alpha$ -grid was initially set forth in the literature (Sec. 2.11), and which require no HF corrections at all, accurately fall on the grid.

#### 0.4 The $\alpha^4$ “Lifetime Desert” between Unpaired and Paired Quark Decays

If Fig. 0.1.11 is examined in detail, it can be seen that the lifetime quark patterns on the  $\alpha$ -grid lines  $x_i \cong 0, 1$  and  $2$  are approximately repeated on the  $\alpha$ -grid lines  $x_i \cong 4, 5$  and  $6$ . This result is brought out in more detail in Fig. 0.1.13, which shows just the 36 threshold-state particles with lifetimes

The lifetimes in Fig. 2.1.1 are plotted on a logarithmic abscissa in order to compress them into a single picture, while at the same time keeping the shorter lifetimes separated enough to be visible as distinct entities. In order to get a feel for the great range of lifetimes displayed in Fig. 2.1.1, it is interesting to write down a few lifetimes  $\tau$  in units of zeptoseconds, which we show in Table 2.1.1. To have this great a range of values in one set of physical entities is remarkable, and to be able to measure them [10] over this range is an impressive achievement. In fact, two different methods are used to obtain the lifetimes or mean lives. The six longest lifetimes  $\tau$  in Table 2.1.1 are determined directly from path lengths and known velocities, but the three shorter lifetimes have to be deduced from the mass widths  $\Gamma$  of the resonances. To show how this works out, we take the nine lifetimes of Table 2.1.1 and replot them in terms of their mass widths, using the mass unit  $\Gamma_{zs} = \hbar/1 \text{ zs} = 0.6582 \text{ MeV}$ . This gives the mass width  $\Gamma$  values shown in Table 2.1.2. The three bottom particles in Table 2.1.2 have widths that are wide enough to be easily measured, but the six top particles do not, so direct lifetime measurements are used. The main purpose here in displaying Tables 2.1.1 and 2.1.2 is to illustrate numerically the wide range of values we have to consider when we study the global patterning of elementary particle lifetimes. These global patterns are important, because only by putting all of the particles together in the same plot can we see just what is happening over this vast range of particle lifetimes.

**Table 2.1.1** Some representative elementary particle lifetimes [10] expressed in units of zeptoseconds, where  $1 \text{ zs} = 10^{-21} \text{ sec}$  — a sextillionth of a second. Particles lifetimes greater than 1 zs occur in widely-spaced groups, whereas the shorter lifetimes occur with essentially a continuum of values.

neutron	$\tau = 885,700,000,000,000,000,000$	zs
muon	$\tau = 2,197,000,000,000,000$	zs
$\pi^\pm$	$\tau = 26,033,000,000,000$	zs
$\Xi^-$	$\tau = 163,900,000,000$	zs
$B^\pm$	$\tau = 1,671,000,000$	zs
$\pi^0$	$\tau = 84,000$	zs
$\Upsilon_{1S}$	$\tau = 121.9$	zs
$J/\psi_{1S}$	$\tau = 7.047$	zs
Z	$\tau = 0.00026379$	zs

The evidence for quark substructure may not in fact require powerful new accelerators, but may already be in evidence in the threshold-state lifetimes. If we picture each threshold-state particle as being composed of a small number of mass substates, some of which are annihilated in the particle decay process, then the factors of two can be accounted for in terms of the number of available substate “decay triggers.” But if we picture the masses of the particles as arising mainly from the amorphous “gluon fields” of the quarks, as is assumed in the Standard Model, then it is not immediately evident how such a clear-cut HF granularity can be explained.

The first example of HF structure is shown in Fig. 2.5.1, where the  $K_L^0$ ,  $\pi^\pm$ , and  $K^\pm$  lifetimes are displayed as exponents  $x_i$  on an  $\alpha$ -spaced lifetime grid, with the  $\pi^\pm$  lifetime as the  $x_i = 0$  anchor for the  $\alpha$ -grid. The  $K_L^0/K^\pm$  lifetime ratio is 4.1, which is of interest in itself (Fig. 0.1.6), but the item of real interest is the fact that the  $\pi^\pm$  lifetime is the geometric mean of these lifetimes, as shown in Fig. 2.5.1. In terms of decay “triggers,” we can account for these lifetime ratios by ascribing one, two, and four triggers to the  $K_L^0$ ,  $\pi^\pm$ , and  $K^\pm$  mesons, respectively. The  $\pi^\pm$  meson is a particle–antiparticle-symmetric hadron that is composed of matching 70 MeV particle and antiparticle substates (Sec. 3.3), only one of which is annihilated in the  $\pi^\pm \rightarrow \mu^\pm$  decay process (Sec. 4.3), so the assignment of

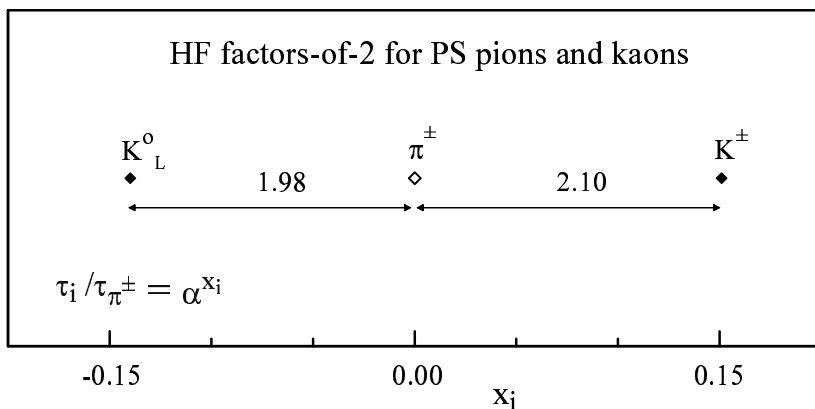


**Fig. 2.5.1** Quantitative factor-of-2 lifetime ratios for the pseudoscalar mesons. The  $K_L^0/K^\pm$  lifetime ratio is 4.13. The  $\pi^\pm$  lifetime, which bears no obvious relationship to these two kaon lifetimes, is almost at their geometric mean, so that the  $K_L^0$ – $\pi^\pm$ – $K^\pm$  triad consists of two factor-of-2 lifetime steps. This suggests that these particles are composed of related mass sub-elements which generate one, two, and four decay “triggers,” respectively, and thus create this HF hyperfine lifetime structure.

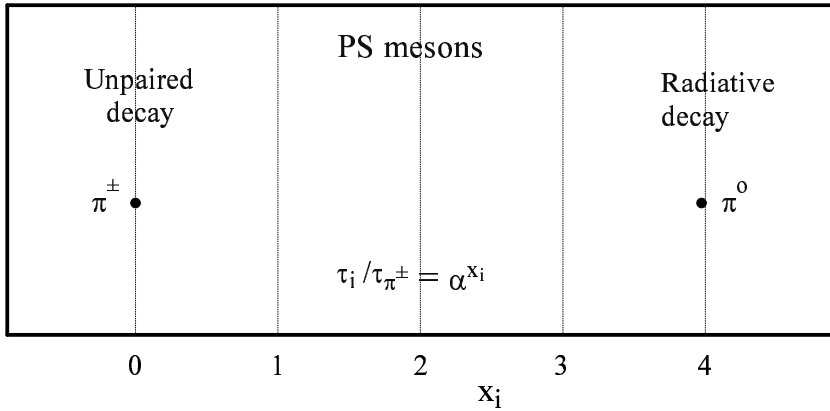


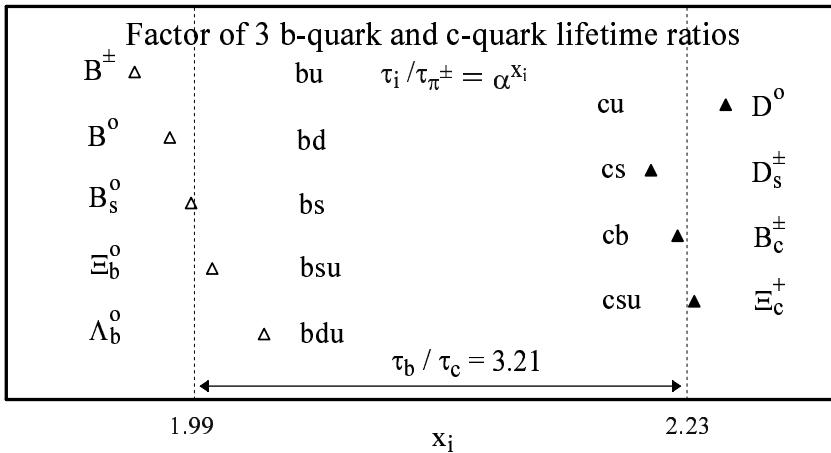
**Fig. 2.8.1** A factor of  $\alpha^4$  spacing between the unpaired-quark lifetime of the  $\pi^\pm$  and the radiative decay of the  $\pi^0$ . The  $\pi^\pm$  meson is composed of matching spinless 70 MeV particle and antiparticle substates. In the decay process, one of these substates is annihilated and the other is set into full relativistic rotation with a calculated spin of  $\frac{1}{2}\hbar$  (Sec. 4.3). It also acquires the charge of the  $\pi^\pm$ , and is converted into a weakly interacting muon. The  $\pi^0$  radiative decay involves the annihilation of both 70 MeV substates, and it proceeds a factor of  $\alpha^4$  faster than the unmatched quark decay of the  $\pi^\pm$ .

$\pi^0$  neutral meson decay is into two gamma rays, and it clearly involves the annihilation of quark–antiquark mass quanta. The  $\pi^\pm$  decay is into a charged muon and a muon neutrino. In the decay process one 70 MeV mass quantum is annihilated, and the remaining one is set into rotation at the relativistic limit, where it has a calculated mass of 105 MeV and a spin angular momentum of  $1/2 \hbar$  (Sec. 4.3). A spin-1/2 neutrino is also produced. The electric charge of the two quarks states in the  $\pi^\pm$  pion is transferred to the spin 1/2 final-state 105 MeV mass quantum, which then appears as the charged  $\mu^\pm$  muon. From the lifetime ratios of 4:2:1 for the  $K_L^0, \pi^\pm, K^\pm$  multiplet shown in Fig. 2.5.1, we conclude that the  $\pi^\pm$  pion has two decay triggers, which suggests that either of the two mass quanta in the  $\pi^\pm$  initial state can trigger the decay. It then follows that the  $\pi^0$  also has two decay triggers, since its lifetime is accurately scaled by a factor of  $\alpha^4$  with respect to the lifetime of the  $\pi^\pm$ .

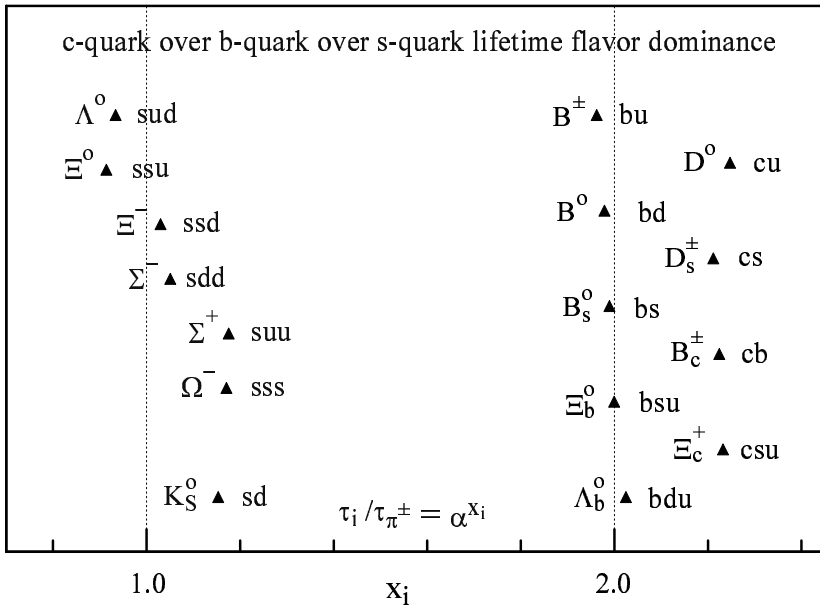
Figure 2.8.2 shows the lifetime  $\alpha$ -plot for the  $\Sigma^+, \Sigma^0$  and  $\Sigma^-$  baryons. The strange  $\Sigma^+$  and  $\Sigma^-$  hyperons decay down to the nonstrange  $p$  and  $n$  nucleons, which is a strangeness-breaking process that leads to long lifetimes for these excitations. The strange  $\Sigma^0$  hyperon decays down to the strange

Fig. 2.9.1, where the five observed  $b$ -dominant states, which do not require HF corrections, are plotted together with the four observed  $c$ -dominant states that also do not require HF corrections. Thus HF corrections play no role in this systematics. The five  $b$ -quark states have an average  $x_i$  value of 1.99 in this standard  $\alpha$ -grid plot, and the four  $c$ -quark states have an average  $x_i$  value of 2.23. The lifetime ratio of these two average values is 3.21. Thus the  $b$ -quark resonances have an average lifetime that is just over a factor of 3 longer than the  $c$ -quark resonances. This factor-of-3 difference between the *unpaired*  $b$  quark and  $c$  quark lifetimes is also observed in the *paired*  $b\bar{b} = \Upsilon$  and  $c\bar{c} = J/\psi$  lifetimes, as displayed in Figs. 0.1.11 and 2.11.10, but the slopes of the lifetime groups make it difficult to evaluate “average lifetimes” for each of these groups, and thus determine an average lifetime ratio for paired excitations.

In order to ascertain how this  $b$ -quark to  $c$ -quark lifetime difference carries over to the masses of these states, we use an  $\alpha$ -grid *lifetime* plot along the *abscissa* and a linear *mass* plot along the *ordinate*, which gives the results displayed in Fig. 2.9.2. The open circles and triangles denote



**Fig. 2.9.1** A plot of the five measured  $b$ -quark meson and baryon lifetimes, shown together with the four  $c$ -quark meson and baryon lifetimes that do not require HF corrections. The vertical lines represent the “group-average” lifetimes. The  $b$ -quark to  $c$ -quark lifetime ratio is 3.21, which is roughly equal to the  $\Upsilon_{1S}/(J/\psi)_{1S} \equiv b\bar{b}/c\bar{c}$  mass ratio of 3.05 (Fig. 2.9.2). Interestingly, the higher-mass  $b$ -quark states have the longer lifetimes. The  $\pi^\pm$  lifetime anchors the global  $\alpha$ -grid for this plot and that of Fig. 2.9.2.



**Fig. 2.10.1** A lifetime plot of unpaired-quark mesons and baryons near  $x_i = 1$  and 2 on the  $\alpha$ -spaced lifetime grid. (The  $K_S^0$  meson is shown here for illustrative purposes with its  $s\bar{d}$  Standard Model quark assignment, but this is not the constituent-quark assignment that is given, e.g., in Table 0.10.1.) No lifetime HF corrections have been applied to the  $x_i \cong 1$  states, and only the  $c$ -quark states near  $x_i = 2$  that do not require HF corrections are included. As can be seen, all of the particles that contain  $c$  quarks have the  $c$  lifetime; the particles that contain a  $b$  quark but no  $c$  quark have the  $b$  lifetime; and the particles that contain an  $s$  quark but no  $b$  or  $c$  quarks have either the  $x_i \cong 1$  or  $x_i \cong 0$  (not shown) lifetime. Thus there is a  $c > b > s$  lifetime flavor dominance.

all approximately equal, and their  $x_i$  values correspond to  $c$ -quark decays. Thus we have clear-cut lifetime quark priorities:

*The lifetime flavor dominance for unpaired quarks is  $c > b > s$ .*

The  $B_c^\pm$  meson is denoted as a  $B$  meson by the Particle Data Group because its mass value reflects the large mass of the  $b$  quark. But if we made lifetimes the primary consideration, we would label it as a  $D_b^\pm$  meson.

It is interesting to consider the effect on particle lifetimes that is achieved by actually replacing one quark flavor with another. Figure 2.10.2 shows two examples where an  $s$  quark is replaced by a  $b$  quark:  $\Xi^0 \rightarrow \Xi_b^0$  and

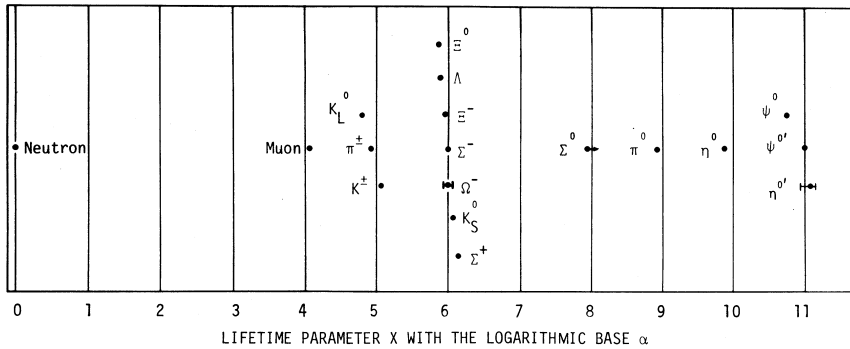


**Fig. 2.11.6** A 1976 lifetime  $\alpha$ -grid plot [46] of the 13 threshold-state particles of Figs. 2.11.2–2.11.4 plus the  $J/\psi$ ,  $\psi'$ ,  $\eta$  and  $\eta'$  mesons, with the neutron as the reference lifetime. The new particles occupy the previously empty  $X = 10$  and 11  $\alpha$ -grid levels.

after the subsequent discoveries of the unpaired  $c$ -quark  $D$  mesons and charmed hyperons, and also the closely-related  $b$ -quark states, which all follow the  $\alpha^4$  separation rule between unpaired-quark and paired-quark decays (Figs. 0.1.13, 0.1.14, 2.8.7 and 2.8.8).

The effect of adding the  $J/\psi$ ,  $\psi'$ ,  $\eta$  and  $\eta'$  mesons to the previous collection of threshold states was evaluated by repeating the ADI-type analysis of Fig. 2.11.3, where no HF corrections are applied. The results are shown in Fig. 2.11.7 [47]. The narrowest and best-centered deviation plot  $R_{\text{exp dev}}$  was again obtained for the scaling factor  $S = 137$ , demonstrating that the four new meson states are in good agreement with the threshold-state lifetime  $\alpha$ -quantization defined by the original thirteen meson and baryon states.

A reference to these lifetime results is contained in Barrow and Tipler's 1986 book *The Anthropomorphic Cosmological Principle*, which contains the following comment:

*Mac Gregor's correlation between powers of  $\alpha$  and the lifetimes of metastable states is another curious trend. [48]*

The 1990 publication update of  $\alpha$ -quantized threshold-state elementary particle lifetimes [49] includes new  $\Upsilon_1$ ,  $\Upsilon_2$  and  $\Upsilon_3$  Upsilon  $b\bar{b}$  resonances, a single (undifferentiated) unpaired  $b$ -quark  $B$  meson, the unpaired  $c$ -quark  $D^\pm$ ,  $D^0$ ,  $D_s$ ,  $\Sigma_c^+$  and  $\Lambda_c^+$  mesons and baryons, the  $\tau$  lepton, and also (finally) a lifetime value for the  $\Sigma^0$ . Figure 2.11.8 gives an  $\alpha$ -grid plot of all the measured elementary particle lifetimes, with the muon now used as

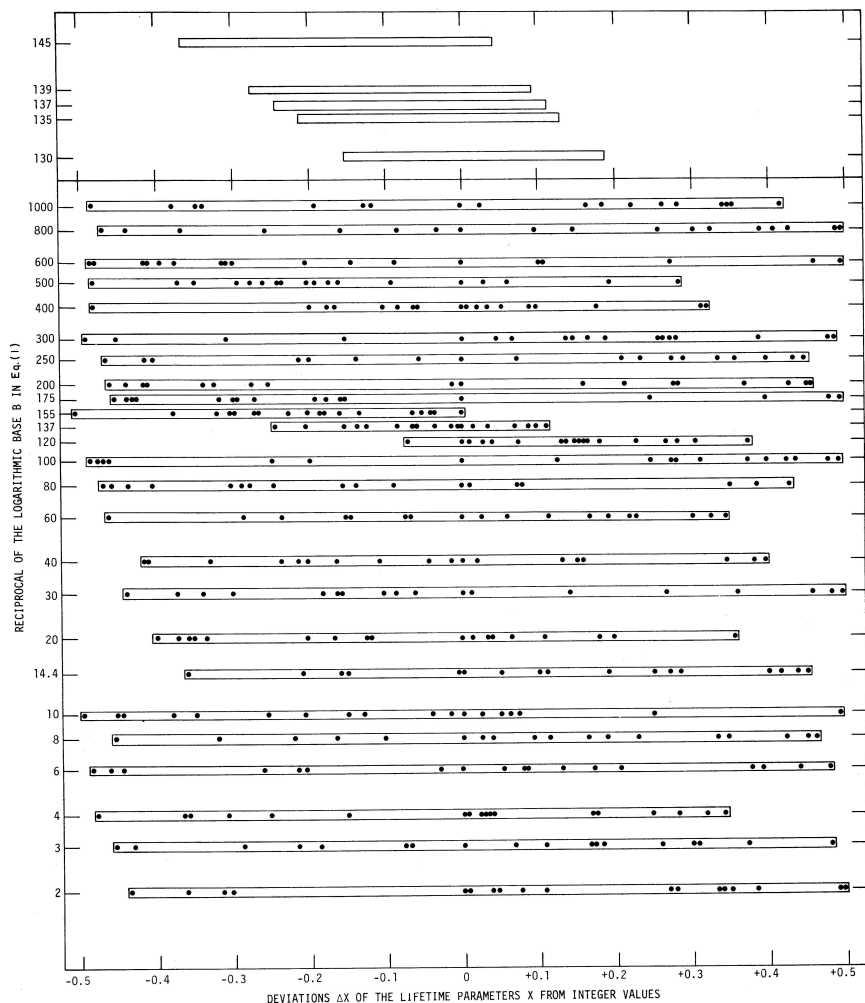


**Fig. 2.11.7** This is a 1976 update [47] of the 1974 ADI type of exponent deviation analysis shown in Fig. 2.11.3, with the  $J/\psi$ ,  $\psi'$ ,  $\eta$  and  $\eta'$  mesons added in. The range of exponent deviations  $R_{\text{exp dev}}$  is narrowest and best centered for the lifetime scaling factor  $S = 137$ .

the reference lifetime [49]. The filled circles denote the original 13 long-lived threshold-state particles of the 1970 compilation (top of Fig. 2.11.1), the open circles denote the threshold-state particles that have subsequently been added, and the dots show the short-lived excited-state particles.

### 3.13 The Fundamental “ $M_X$ Octet” of Threshold-State Particles

In Sec. 3.6 we listed the 36 long-lived elementary particles that exhibit  $\alpha$ -quantized lifetimes (Chapter 2). We then added in the stable electron and proton, and also the  $\phi$  meson, whose decay into a  $K\bar{K}$  pair of equal strangeness leads to an anomalously short lifetime. We subtracted the  $\Xi_b$  baryon. This list is displayed in Table 3.6.1, where the 38 particles are sorted into “generations” that correspond roughly to their “hierarchy” in the mass generation process. The particles in the first generation are the non-strange bosons (PS mesons) in group (1a) and the fermions (leptons and nucleons) in group (1b) of Table 3.6.1. The second generation particles are the strange bosons and fermions, which are separated into a low-mass tier of spin-0 (PS mesons) and spin-1 (phi meson) bosons that comprise groups (2a) and (2b), respectively, and a higher-mass tier of hyperons that comprise group (2c). The third and fourth generations are the charm and bottom particle states, respectively. The particles that appear in the excitation towers of Secs. 3.7–3.12 are those in groups (1a), (1b), (2a) and (2b), which are the ones of greatest interest from the standpoint of studying the  $\alpha$ -quantization of elementary particle masses. In the calculation of particle masses we use the charge-independent (CI) masses  $\pi = 1/2 (\pi^\pm + \pi^0)$  and  $K = 1/2 (K^0 + K^\pm)$  to represent the pions and kaons (Sec. 3.14), and we use the proton itself to represent the proton-neutron “nucleon” pair. These group 1(a), 1(b), 2(a) and 2(b) particle states form the “ $M^X$  octet”, with the electron mass serving as the reference mass for the octet.

Before listing the  $M^X$  octet particles, we first briefly recapitulate the  $M^X$  production process. When a symmetric  $m_b\bar{m}_b$  or  $m_f\bar{m}_f$  two-electron  $\alpha$ -leap is generated from an electron-positron pair, the resulting energy level acts as an  $M_\pi$ ,  $M_\phi$  or  $M_{\mu\mu}$  platform mass upon which further excitations can be made (Eqs. (3.5.5)–(3.5.7)). Asymmetric one-electron  $\alpha$ -leaps can also be identified that exist as components of the symmetric production process, and they lead to the asymmetric platform masses  $M_K$  and  $M_\mu$  (Eqs. (3.5.9) and (3.5.8)). We might logically expect that subsequent excitations of the  $M_K$  and  $M_\mu$  platform masses would be in single  $\alpha$ -leaps of  $m_b = 70$  MeV or  $m_f = 105$  MeV, respectively, and that excitations of the  $M_\pi$ ,  $M_\phi$  and  $M_{\mu\mu}$  platform masses would be in double  $\alpha$ -leaps of  $m_b\bar{m}_b = 140$  MeV or  $m_f\bar{m}_f = 210$  MeV. Instead, what we find is that the subsequent excitations of all five of these platform masses are in units of the supersymmetric “multiple- $\alpha$ -mass” quantum

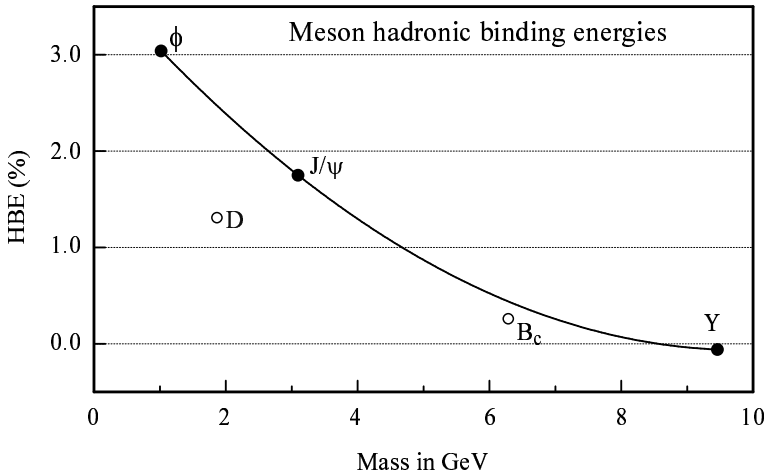


**Fig. 3.17.2** Hadronic binding energies for the  $\phi \equiv s\bar{s}$ ,  $J/\psi \equiv c\bar{c}$  and  $\Upsilon \equiv b\bar{b}$  resonances. These binding energies are obtained by starting with the low-energy  $\alpha$ -masses and platform states defined in Secs. 3.4 and 3.5, extrapolating these masses all the way up to the  $\Upsilon$  meson, and comparing the calculated unbound masses of these states with the experimental masses (Table 3.15.1 and Eq. (3.15.1)). These three binding energies define the curve in Fig. 3.17.2, which is an eyeball fit to the data. As can be seen, the binding energy (percentagewise) goes essentially to zero at the energy of the  $\Upsilon$ . Also shown are the binding energies of the  $D \equiv q\bar{c}$  meson ( $q \equiv u, d$ ) and the  $B_c \equiv b\bar{c}$  meson (whose mass has recently been accurately measured [56]). As discussed in the text, the decrease in HBE values shown in Fig. 3.17.2 can plausibly be regarded as a manifestation of “asymptotic freedom”.

3.5, and were deduced from the masses of the lowest elementary particle states — the electron, pion and muon “Rosetta stones” of Sec. 3.3. We use multiples of these same low-energy masses to reproduce other particle masses all the way up to the  $\Upsilon(9460)$  meson, which is almost two orders of magnitude higher in energy. It then turns out that the hadronic binding energy that we need to empirically apply to these  $s\bar{s} \rightarrow c\bar{c} \rightarrow b\bar{b}$   $M^T$  basis states in order to reproduce their experimental values systematically decreases from 3.04% to 1.75% to  $-0.06\%$ , as is displayed in the HBE curve in Fig. 3.17.2, and listed in Table 3.15.1. This suggests that the HBE is proportional to the charge states (which are not proportional to the masses), so that the HBE essentially vanishes (percentagewise) at the higher mass values. Two more high-mass data points we can add in here come from the  $D = q\bar{c}$  meson, ( $q \equiv u, d$ ), whose averaged HBE is 1.31%, and the  $B_c = b\bar{c}$  meson (whose mass has recently been measured with high accuracy

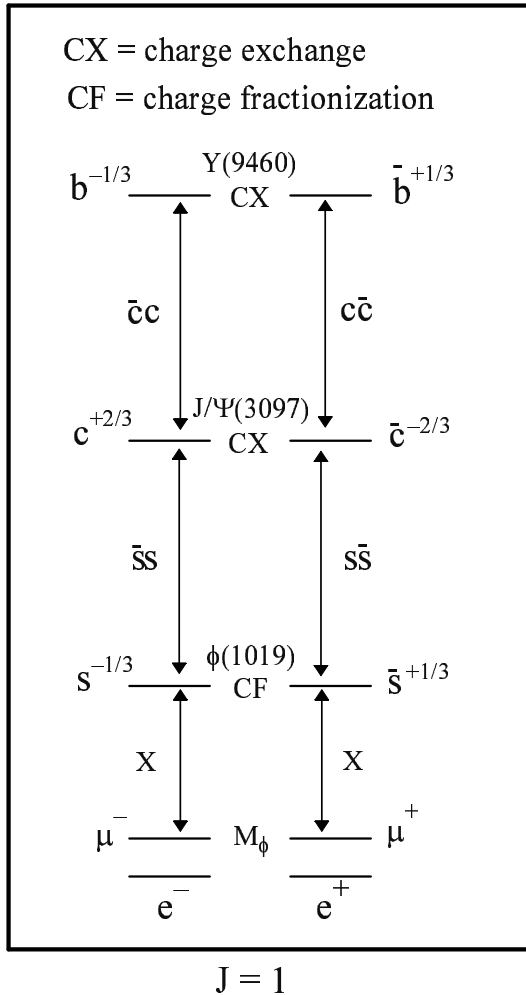


**Fig. 3.18.1** The  $M^T$   $s$ ,  $c$ ,  $b$  mass-tripling excitation tower of Fig. 3.17.1, shown schematically separated into its particle and antiparticle components. An  $XX$  excitation of the  $M_\phi$  platform state leads to the generation of a  $\phi \equiv s\bar{s}$  quark pair (see Fig. 3.12.3), where charge fragmentation (CF) creates  $e = (-1/3, +1/3)$  charges on the  $s$  and  $\bar{s}$  quarks, respectively. The resulting quark gluon field produces a hadronic binding energy of 3% (Table 3.15.1). Then two successive mass-triplings of the  $\phi$  accurately reproduce the  $J/\psi \equiv c\bar{c}$  and  $\Upsilon \equiv b\bar{b}$  masses (Fig. 3.17.3). These sequential  $M^T$  excitations are accompanied by a CX charge exchange  $e$  for the  $J/\psi$  and then a reverse CX charge exchange  $-e$  for the  $\Upsilon$ , which create the charges  $e = (+2/3, -2/3)$  on the  $c$  and  $\bar{c}$  quarks, and  $e = (-1/3, +1/3)$  on the  $b$  and  $\bar{b}$  quarks.

seven  $m_b$  subquanta, as shown in Fig. 3.25.2, and the manner in which the particle–antiparticle asymmetry of these seven substates is reflected in the strangeness quantum number that it carries is not immediately apparent. But we can assume for the sake of argument that it is carried in the  $\pi_4$  quark state of Fig. 3.25.2, and that the higher-mass  $s$  quark in the  $\Sigma$  hyperon is created as a hybrid excitation by adding a 280 MeV “strange”  $\pi_4$  quark to a  $q$  quark, thus creating a strange quark hybrid excited-state  $s^* = 595$  MeV. Since we are dealing here with the phenomenology of mass values, our best clue to as to what is actually going on resides in the mass fits that we can obtain with this kind of reasoning. If we accept the existence of the strange quarks  $s = 525$  MeV and  $s^* = 595$  MeV, we can construct the hyperon ground states as the quark configurations  $\Lambda = qqs$ ,  $\Sigma = qqs^*$ ,  $\Xi = qss$  and  $\Omega = ss^*s^*$ . These give the hyperon masses displayed in Fig. 3.26.3, which obey an extended 210 MeV and 280 MeV “two-strange-quark” interval rule. The  $\alpha$ -quantized constituent-quark approach that forms the basis for the present work does not seem consistent with “nuclear-physics-type” spin-orbit or other mass splitting mechanisms, so the  $s$  and  $s^*$  “two-mass” strange quark emerges as the most logical resolution of the  $\Lambda$ – $\Sigma$  mass-splitting problem.

There is one other particle — the  $K^*(892)$  meson — that seems to clearly require the  $s^* = 595$  MeV hybrid strange quark. The  $K^*$  has an isotopic-spin-averaged mass of 894 MeV [Appendix B]. From its spin value  $J = 1$ , we know that the  $K^*$  is necessarily composed of a pair of spin-1/2 quarks. The quark assignment  $K^* = q(315) + s(525) = K^*(840)$  is too low in mass by 54 MeV. The alternate assignment  $K^* = q(315) + s^*(595) = K^*(910)$  gives a  $K^*$  meson with a hadronic binding energy of 16 MeV, or 1.8%, which is comparable to the hadronic binding energies displayed in Table 3.15.1. The reason for the anomalously high value (by 70 MeV) of the  $K^*$  may lie in its  $M_K$  platform production mechanism, which is displayed in Fig. 0.2.20 and discussed in Sec. 0.9. Two  $M_K$  platform excitations shown there are  $K = m_bX$  and  $K^* = m_bXX$ . The spin-0  $K$  meson can be constructed of spinless pion quarks, but the spin-1  $K^*$  meson requires spin-1/2 muon quarks. The  $XX$  platform excitation can be written in a variety of isoergic forms, but the  $K^*$  requires it to be written as  $XX = q\bar{s}$  or  $\bar{q}s$ . The  $K^*$  itself is then  $q\bar{s}m_b \equiv q\bar{s}^*$  or  $\bar{q}s m_b \equiv \bar{q}s^*$ . Since the  $K^*$  is the lowest-mass *strange* spin-1 particle, its mass value is of particular phenomenological significance. The  $K^*$  isotopic-spin mass splitting of 4.44 MeV closely resembles that of the pions and kaons in magnitude, and the  $K^{*0}$ , like the  $K^0$ , has the heavier mass. So the  $K$

**Table 4.3.1** Mechanical properties of the fully relativistic spinning sphere (RSS), whose equator is moving at, or infinitesimally below, the velocity of light,  $c$  (Eq. (4.3.1)). Assuming this limiting rotation, we set forth the following four lemmas.

Lemma 1: The mass of an RSS is half again as large as that of its nonspinning counterpart:  $M_s = \frac{3}{2}M_0$ .

Lemma 2: The volume of an RSS is half again as large as that of its nonspinning counterpart:  $V_s = \frac{3}{2}V_0$ .

Corollary A: The density distribution  $\rho(r) = m(r)/v(r)$  of an RSS is an invariant, independent of its rotational velocity.

Corollary B: Since the density distribution  $\rho(r)$  of a massive object is a measure of its applied stresses, the invariance of  $\rho(r)$  can be taken as an indication of the absence of relativistic stresses.

Corollary C: An RSS point-event described in laboratory ( $K$ ) and rotating frame ( $K'$ ) coordinates gives  $r = r'$ ,  $v = v'$ ,  $\omega = \omega'$  and  $a = a'$  for the radius, azimuthal and angular velocities, and radial acceleration, respectively.

Lemma 3: The calculated moment of inertia of an RSS is  $I = \frac{1}{2}M_sR_s^2$ , where  $R_s$  is the radius of the sphere.

Lemma 4: If the RSS radius is the Compton radius  $R_s = \hbar/M_sc$ , then its calculated spin angular momentum is  $J_s = \frac{1}{2}\hbar$ .

integration in Eq. (4.3.5) gives  $I_s = \frac{3}{4}M_0R_s^2 = \frac{1}{2}M_sR_s^2$ , Lemma 3. Finally, inserting the Compton radius  $R_s = \hbar/M_sc$  and setting  $\omega R_s = c$  gives  $J = I_s\omega = \frac{1}{2}\hbar$ , Lemma 4. If the equatorial velocity  $\omega R_s$  of the spinning sphere is infinitesimally less than  $c$ , then the corrections to the relativistic equations are also infinitesimal.

Corollaries A, B, and C suggest that the relativistic stresses which are customarily assumed to apply to a relativistically spinning sphere [87–89] may not be a factor. For example, the relativistic stretching of the length of a string has been pointed out [88], but the corresponding increase of the mass of the string so that its mass per unit length remains invariant [86] was apparently overlooked.

The relevance of this RSS model to the  $\alpha$ -quantization of particle masses is that it ties together the  $J = 0$  and  $J = 1/2$   $\alpha$ -mass excitation quanta  $m_b$  and  $m_f$  as rotationless and rotational states of the same basic spherical mass quantum,  $m_b = m_e/\alpha = 70.025$  MeV. The supersymmetric “crossover” excitation quantum  $X = 6m_b = 4m_f = 420.15$  MeV (Sec. 3.9) is the lowest-mass excitation unit that can produce  $m_b \leftrightarrow m_f$  transformations which are both isoergic and particle–antiparticle-symmetric. These transformations

where the mass-energy term  $mc^2$  is in units of MeV. If we take  $mc^2$  to be the average pion mass,  $\bar{\pi} = 137.27$  MeV, we obtain a pion Compton radius  $r$  of 1.438 fermi. This value for  $r$  gives an electrostatic energy  $e^2/r$  in Eq. (6.1.3) of 1.001 MeV. This value is about 2% below the energy of an unbound electron–positron pair, and it reflects the  $\sim 2\%$  hadronic binding energy in the pion (see Sec. 3.15). We have thus tied together the mass of the particle–anti-particle–symmetric pion with the mass of a particle–anti-particle–symmetric electron–positron pair. According to the present-day paradigm of the Standard Model, these two masses should be unrelated.

The calculation of the “intrinsic” mass of the pion that should be inserted into Eq. (6.1.5) is obscured by both binding energy and isotopic spin mass-splitting effects. If we use the  $\pi^\pm$  mass in Eq. (6.1.5), we obtain a pion Compton radius of 1.414 fermi, which gives an electrostatic energy in Eq. (6.1.3) of 1.019 MeV. This differs from the 1.022 MeV rest-mass energy of an electron–positron pair by just 0.3%. (If we insert the muon mass into Eq. (6.1.5), the resulting radius is 1.868 fermi, which is equal to  $2/3$  of the classical electron radius  $R_0 = e^2/m_e c^2 = 2.818$  fermi, to an accuracy of 0.7%.) The main point we are making in this calculation is not about precise numerical values, but rather about the fact that by combining the fine structure constant  $\alpha = e^2/\hbar c$  with the Compton radius  $r = \hbar/mc$ , we obtain a theoretical expression (Eq. 6.1.3) that ties together the mass of the pion with the mass of an electron pair. This point is of interest in connection with the definition of the fundamental mass excitation  $m_b = m_e/\alpha = 70.025$  MeV in Eq. (3.4.1). But it is also of interest with respect to the definition of the constant  $\alpha$ . We can rewrite Eq. (6.1.3) in the form

$$(e^2/r)/(mc^2) \cong (1/137). \quad (6.1.6)$$

We now have the numerical factor  $\sim 1/137$  expressed as the ratio of an electrostatic energy divided by a mass energy — an electric charge energy over a pion energy, where the electrostatic term consists of two electric charges  $e$  separated by a Compton radius  $r$  that corresponds to the mass of the pion. This suggests that the factor  $\sim 1/137$  is in some manner related to the “geometries” of both an electron charge pair and a pion, where this “geometry” can be a function of charge structures or mass structures or both. Thus the theoretical explanation for the numerical value  $\sim 1/137$  must come from a clear understanding of particle mass structure and charge structure.

then applying an additional compression factor of  $(1 + 3/2\alpha)$ , where the conversion to “spinless muon matter” or “pion matter” takes place. The  $J = 0$   $\alpha$ -mass  $m_b$  is in essence the mass of a “non-spinning muon.” It is the non-spinning form of the  $J = 1/2$   $\alpha$ -mass  $m_f$ .)

*Scenario 2B* is a somewhat different route to the same conclusion. Our starting point here is the electron that was produced in Scenario 1, which has mass  $m_e$  and Compton radius  $R_C = 3.86 \times 10^{-11}$  cm. We assume as an *ansatz* that “electron mechanical matter” is compressible, and that its compressed energy varies inversely with its radius, just as the self-energy of the electrostatic field does. We then compress it down to the radius  $R_e = R_C/(1 + 3/2\alpha)$ , so that its energy is increased to  $m_e(1 + 3/2\alpha)$ . At that critical point the “electron mechanical mass” is converted into “muon mechanical mass,” which is stable at the higher mass density of the muon. The Compton radius of the muon is the same as the compressed radius of the electron, so the electron-to-muon mass transformation is accomplished with no change in the size of the system.

The Scenario 2 electron-to-muon conversion process, in either its 2A or 2B form, corresponds to the “ $\alpha_2 \equiv \alpha_\mu$ ” phase transition, which produces the muons,  $m_\mu \cong m_f + m_e$  and  $\bar{m}_\mu \cong \bar{m}_f + \bar{m}_e$ , and also the pion,  $m_\pi \cong m_b + m_e + \bar{m}_b + \bar{m}_e$ . This  $\alpha$ -generation process is successively repeated in the creation of the  $u$ ,  $d$ ,  $s$ ,  $c$ ,  $b$  quarks and antiquarks as multiples of the  $m_f$  and  $\bar{m}_f$  masses (Figs. 0.2.4, 0.2.5 and 0.2.23), the creation of the pseudoscalar mesons as multiples of the  $m_b$  and  $\bar{m}_b$  masses (Figs. 0.2.11 and 0.2.24), and the creation of hybrid excitations such as the  $K^*$  meson and  $\Sigma$  hyperons (Sec. 3.26), which contain both  $m_f$  and  $m_b$  mass units.

Scenario 3 involves the Standard Model  $u$  and  $d$  quarks, which have equal masses in our isotopic-spin-averaged constituent-quark mass formalism. We denote these collectively as  $q \equiv (u, d)$  “nucleon quarks,” since these  $q$  quarks reproduce the proton and neutron — the two nucleon states. The  $q$  quarks form the “ground state” for an additional mass  $\alpha$ -enhancement by a factor of  $1/\alpha$ , which increases their masses by a factor of 137 and boosts them into the realm of the ultramassive  $W$  and  $Z$  gauge bosons and top quark  $t$ . This *second-order*  $\alpha$ -leap (the *first-order*  $\alpha$ -leap was from the electron to the muon and then to the  $u$  and  $d$  quarks) generates the  $\alpha$ -quarks  $q^\alpha \equiv (u^\alpha, d^\alpha) = q/\alpha \equiv (u, d)/\alpha$ . These  $q^\alpha$  quarks reproduce the  $W$ – $Z$  average mass and the top quark mass (Secs. 0.10 and 3.20). The phase transition  $\alpha_3 = \alpha_q$  takes place during proton–anti-proton collisions at the Fermilab tevatron. A proton and an antiproton collide at energies of 1 TeV each. At these energies, the three  $q$  quarks inside the proton and the three

	Mean life $\tau$ (sec)	Full width $\Gamma$ (MeV)	Particle
<b>Eleven strange kaons <math>K</math></b>			
77	1.3021E-23	5.0550E+01	$K^*$ (892)
78	7.3135E-24	9.0000E+01	$K_1$ (1270)
79	3.7828E-24	1.7400E+02	$K_1$ (1400)
80	2.8371E-24	2.3200E+02	$K^*$ (1410)
81	2.2697E-24	2.9000E+02	$K_0^*$ (1430)
82	6.3442E-24	1.0375E+02	$K_2^*$ (1430)
83	2.0441E-24	3.2200E+02	$K^*$ (1680)
84	3.5388E-24	1.8600E+02	$K_2$ (1770)
85	4.1397E-24	1.5900E+02	$K_2^*$ (1780)
86	2.3848E-24	2.7600E+02	$K_2$ (1820)
87	3.3243E-24	1.9800E+02	$K_4^*$ (2045)
<b>Thirteen charm mesons <math>D</math> and <math>\psi</math></b>			
88	3.2265E-23	2.0400E+01	$D_1(2420)^0$
89	2.6328E-23	2.5000E+01	$D_1(2420)^\pm$
90	1.8284E-23	3.6000E+01	$D_2^*(2460)$
91	4.3881E-23	1.5000E+01	$D_{s2}(2573)^\pm$
92	6.3290E-23	1.0400E+01	$\chi_{c0}(1P)$
93	7.3956E-23	8.9000E-01	$\chi_{c1}(1P)$
94	3.1952E-23	2.0600E+00	$\chi_{c2}(1P)$
95	4.7015E-23	1.4000E+01	$\eta_c(2S)$
96	2.8618E-23	2.3000E+01	$\psi(3770)$
97	2.2697E-23	2.9000E+01	$\chi_{c2}(2P)$
98	8.2276E-24	8.0000E+01	$\psi(4040)$
99	6.3904E-24	1.0300E+02	$\psi(4160)$
100	1.0616E-23	6.2000E+01	$\psi(4415)$
<b>Three bottom mesons <math>\Upsilon</math></b>			
101	3.2108E-23	2.0500E+01	$\Upsilon(4S)$
102	5.9837E-24	1.1000E+02	$\Upsilon(10860)$
103	8.3318E-24	7.9000E+01	$\Upsilon(11020)$
<b>Thirteen nonstrange baryons <math>N</math></b>			
104	2.1940E-23	3.0000E+02	$N(1440)P_{11}$
105	5.7236E-24	1.1500E+02	$N(1520)D_{13}$
106	4.3881E-24	1.5000E+02	$N(1535)S_{11}$

	Mean life $\tau$ (sec)	Full width $\Gamma$ (MeV)	Particle
<b>Thirteen nonstrange baryons <math>N</math> (Cont.)</b>			
107	3.9892E-24	1.6500E+02	$N(1650)S_{11}$
108	4.3881E-24	1.5000E+02	$N(1675)D_{15}$
109	5.0632E-24	1.3000E+02	$N(1680)F_{15}$
110	6.5821E-24	1.0000E+02	$N(1700)D_{13}$
111	6.5821E-24	1.0000E+02	$N(1710)P_{11}$
112	3.2911E-24	2.0000E+02	$N(1720)P_{13}$
113	1.3164E-24	5.0000E+02	$N(2190)G_{17}$
114	1.6455E-24	4.0000E+02	$N(2220)H_{19}$
115	1.3164E-24	5.0000E+02	$N(2250)G_{17}$
116	1.0126E-24	6.5000E+02	$N(2600)I_{1,11}$
<b>Ten nonstrange baryons <math>\Delta</math></b>			
117	5.5781E-24	1.1800E+02	$\Delta(1232)P_{33}$
118	1.8806E-24	3.5000E+02	$\Delta(1600)P_{33}$
119	4.5394E-24	1.4500E+02	$\Delta(1620)S_{31}$
120	2.1940E-24	3.0000E+02	$\Delta(1700)D_{33}$
121	1.9946E-24	3.3000E+02	$\Delta(1905)F_{35}$
122	2.6328E-24	2.5000E+02	$\Delta(1910)P_{31}$
123	3.2911E-24	2.0000E+02	$\Delta(1920)P_{33}$
124	1.8284E-24	3.6000E+02	$\Delta(1930)D_{35}$
125	2.3095E-24	2.8500E+02	$\Delta(1950)F_{37}$
126	1.6455E-24	4.0000E+02	$\Delta(2420)H_{3,11}$
<b>Thirteen strange hyperons <math>\Lambda</math></b>			
127	1.3164E-23	5.0000E+01	$\Lambda(1405)S_{01}$
128	4.2193E-23	1.5600E+01	$\Lambda(1520)D_{03}$
129	4.3881E-24	1.5000E+02	$\Lambda(1600)P_{01}$
130	1.8806E-23	3.5000E+01	$\Lambda(1670)S_{01}$
131	1.0970E-23	6.0000E+01	$\Lambda(1690)D_{03}$
132	2.1940E-24	3.0000E+02	$\Lambda(1800)S_{01}$
133	4.3881E-24	1.5000E+02	$\Lambda(1810)P_{01}$
134	8.2276E-24	8.0000E+01	$\Lambda(1820)F_{05}$
135	6.9285E-24	9.5000E+01	$\Lambda(1830)D_{05}$
136	6.5821E-24	1.0000E+02	$\Lambda(1890)P_{03}$
137	3.2911E-24	2.0000E+02	$\Lambda(2100)G_{07}$
138	3.2911E-24	2.0000E+02	$\Lambda(2110)F_{05}$
139	4.3881E-24	1.5000E+02	$\Lambda(2350)H_{09}$

This is a review article that summarizes the experimental evidence for an  $\alpha$ -dependence in the lifetimes and masses of the long-lived threshold-state elementary particles. It is the fore-runner for the book *The Power of  $\alpha$* .

51. *What is the Electron?* V. Simulik (ed.) (Apeiron Press, Montreal, 2005), pp. 129–153. “What causes the electron to weigh?”

This chapter in the book discusses the concept of the mass of the electron.

52. arXiv.org/hep-ph/0603201, 24 March 2006, “The top quark to electron mass ratio  $m_t = 18m_e/\alpha^2$ , where  $\alpha = e^2/\hbar c$ .”

This paper gives the first calculation of the top quark mass as a second-order  $\alpha$ -leap from the mass of the electron. The mass equation shown in the title gives a calculated top quark mass of 172.73 GeV, as compared to the current consensus Fermilab CDF/D0 mass value of  $172.5 \pm 2.3$  GeV.

53. arXiv.org/hep-ph/0607233, 20 July 2006, “A ‘Muon Mass Tree’ with  $\alpha$ -quantized lepton, quark and hadron masses.”

This paper describes the muon and pion “mass trees” that are displayed in Figs. 0.2.23 and 0.2.24 of the present book.

54. Int. J. Mod. Phys. A **22**, 566–569 (2007), “The Phenomenology of  $\alpha$ -Quantized Particle Lifetimes and Masses: Particle Mass Generation without the Higgs.”